# Molecular dynamics investigation of dynamic crack stability

P. Gumbsch
*Max-Planck-Institut für Metallforschung, Institut für Werkstoffwissenschaft, Seestr. 92, 70174 Stuttgart, Germany*

S. J. Zhou* and B. L. Holian
*Theoretical Division and Center for Nonlinear Studies, Los Alamos National Laboratory, Los Alamos, New Mexico 87545*
(Received 22 August 1996)

A series of molecular-dynamics simulations has been performed in order to evaluate the effects of several physical factors on dynamic crack stability. These factors are the crystalline structure and the interatomic interaction modeled by various empirical potentials. For brittle crack propagation at low temperature we find that steady-state crack velocities are limited to a band of accessible values. Increasing the overload beyond $K_{Ic}$, the crack can propagate with a steady-state velocity, which quickly reaches the terminal velocity of about 0.4 of the Rayleigh wave speed. The magnitude of the terminal velocity can be related to the nonlinearity of the interatomic interaction. Further increasing the overload does not change the steady-state velocity dramatically, but significantly increases the amplitude of acoustic emission from the crack tip. Loading the crack even further leads to instabilities which take the form of cleavage steps, dislocation emission, or branching. The instability is closely related to the buildup of a localized coherent, phononlike field generated by the bond-breaking events. The form of the instability depends critically on crystal structure and on the crystallographic orientation of the crack system but can also be correlated with the relative ease of dislocation generation (and motion). [S0163-1829(97)08305-7]

## I. INTRODUCTION

Fracture of materials is essentially a dynamic process, at least in the final stage.[1] Although this last stage of fracture might at first seem rather irrelevant, closer consideration shows that dynamic fracture is also one of the underlying physical processes in the so-called semibrittle fracture regime[2] where materials toughness is governed by the competition of the dynamic atomic bond breaking and dislocation mobility. Semibrittle fracture is usually observed in materials which undergo a brittle-to-ductile transition (below the transition temperature) and consequently we need to develop deeper insight into the dynamic fracture process in order to eventually understand the brittle-to-ductile transition.

Dynamic fracture has been stimulating interest not only because of its fundamental importance in understanding fracture processes and because of practical applications such as engineering design and earthquake prediction, but also because of the challenges to mathematical analyses and experimental techniques. A number of points remain unclear in the description of this dynamic process, especially at the atomistic scale. A very important one is how to understand the consequence of a mechanical overload of the crack, which eventually leads to an instability of the perfectly brittle, atomically sharp crack. In this paper, we will show that understanding complex processes such as crack branching and dislocation emission from a dynamic crack requires realistic treatment of the truly atomistic dynamics, and that different interatomic potentials have a profound effect on the behavior.

Dynamic instability has not been seriously explored due to its highly nonlinear character (see Ref. 1) although Yoffe's analysis[3] implies that the stresses at the crack tip may cause the crack to branch at sufficiently high speeds. This phenomenon has received much attention, following recent experimental studies.[4–7] Langer *et al.*[8] have introduced dissipation into continuum dynamic theory. Lately Ching *et al.*[9] have studied a two-dimensional cohesive-zone model of fracture dynamics and found that moving cracks are strongly unstable against deflection in essentially all conventional cohesive-zone models. They also concluded that quasistatic instability analyses[10] are inherently incapable of detecting dynamic instabilities, even in the quasistatic limit. The failure of continuum instability analyses is not very surprising since lattice features and realistic nonlinearity at the dynamic crack tip are not included. The work of Marder and co-workers[11,12] is a lattice theory. Beyond the instability they find crack branching at a critical velocity. However, the atomic interactions in their model are extremely simplified, so that they cannot realistically treat crack branching and dislocation emission. Xu and Needleman[13] have also investigated crack branching using a finite element continuum computer code, where the continuum is characterized by a material constitutive law relating stress and strain through the tractions and displacement jumps across a specified set of cohesive surfaces at various angles.

The earliest molecular-dynamics (MD) simulations of fracture were carried out some 20 years ago by Ashurst and Hoover [W. T. Ashurst and W. G. Hoover, Phys. Rev. B **14**, 1465 (1976)]. Many of the features of crack propagation at the atomistic level were described therein, including the observation of a steady crack velocity that was 64% of the long-wavelength Rayleigh-wave speed. Their interaction potentials were all harmonic in nature, with varying ranges, but anharmonic effects were not considered except for finite-strain effects. Most importantly, the system sizes studied were exceedingly small (32 atoms wide by 16 high in the

 

direction of propagation, with initial crack lengths of only 10 atoms). As a result, boundary effects were severe, so that reflected sound waves bathed the crack tip in the short time available for steady propagation, due to fixed-grip boundary conditions transverse to the crack advancement direction. Moreover, such short crack lengths require excessive loading to initiate crack motion (so-called lattice trapping). In spite of these severe computational limitations, a veritable goldmine of information was obtained.

With the advance of computer power and efficient MD numerical techniques, the full dynamical and atomistic nature of this problem can be revealed. To understand the complicated processes at the onset of instability, molecular-dynamics simulations need to be both brute force (large scale) and delicate (i.e., carefully initialized for a gently overloaded sharp crack). However, there are two major limitations in investigating dynamic fracture with MD: small computational system sizes and short time scales. The strain fields associated with a crack are long range in character, and the stress waves generated by a propagating crack need special treatment to prevent them from reflecting from free surfaces and returning to disturb the behavior of the crack. An efficient atomistic boundary treatment using ramped viscous damping has been developed to significantly absorb sound waves generated at crack tips.[14] But the time scale is still limited to nanoseconds even with powerful parallel computers, which now allow MD simulations with millions of atoms.[14–16] We have attempted to overcome these constraints by carefully selecting appropriate boundary conditions, which must be mechanically well defined. We have chosen two model geometries which fulfill these requirements. The first method is to embed an atomically sharp equilibrium crack of finite length, which is loaded at the Griffith value in a displacement field according to the continuum elasticity solution for this geometry. By applying a small overstrain we can then gently drive the crack. This method is termed the ''stadium boundary condition'' since the active atomistic region surrounding the crack has the shape of a football stadium. The principal goal of the stadium treatment is to study early-time dynamic behavior of a crack in a pristine bulk sample in a well-controlled way. The second method is to artificially constrain a long crack in a thin strip such that the energy release rate does not depend on crack length and can therefore be controlled during crack propagation.[1,17,18] In this case, the study of steady-state long-time behavior is the primary objective.

The purpose of this paper is to determine the energy dissipating processes during the propagation of a perfectly brittle crack as well as at the instability. We aim at identifying certain generic mechanisms at the simplest level rather than providing results at the highest possible level of accuracy for one particular material. We expect that the results obtained here will also be useful for analyzing experimental data. Dynamic fracture experiments are very difficult to perform; to date, no truly atomistic, time-resolved measurements have been made. Our intention is to fill in this particular gap, in lieu of such experimental information. Atomistic computer experiments can, indeed, provide such unavailable information, both to those who might design future lab experiments and to engineers who might design constitutive models of dynamic fracture.

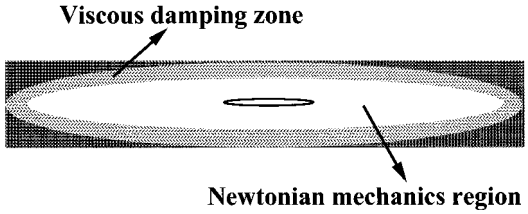


FIG. 1. Schematic of the ''stadium'' computational cell.

## II. COMPUTATIONAL METHODS

We have chosen to study different crystal structures [the two-dimensional (2D) triangular lattice and the face-centered-cubic (fcc) crystal structure] and two different loading conditions (the ''stadium boundary conditions'' and the ''strip geometry'') in order to vary the observable mechanisms to the largest possible extent. We then extract the differences and the common features from the different models. It turns out that the comparison of different models can actually reveal the important processes necessary for the understanding of the complex fracture phenomena which occur during dynamic crack propagation.

### A. Stadium boundary conditions

In the work reported here, the stadium boundary conditions were only used in 2D (though extension to 3D is straightforward). The computational cell with a sharp equilibrium crack and viscous damping boundaries is depicted in Fig. 1. The system consists of rectangular samples with an aspect ratio of about 5 or 6. Ensembles of more than 400 000 atoms ($\sim 240 r_0 \times 1440 r_0$, where $r_0$ is the nearest-neighbor distance of the 2D triangular lattice), are sufficiently large to take care of the long-range character of crack strain fields. The shortest half-length of the crack is $240 r_0$, which is long enough that the waves generated at one crack tip cannot reach the other crack tip before an instability event has occurred. If stress waves generated by a propagating crack bounce back from free surfaces, they can severely disturb the behavior of the crack, including causing crack arrest, as shown by Holian and Ravelo.[14] Consequently, we absorb waves and mobile dislocations in a smooth way by ramping up viscous damping in a region surrounding the central elliptical sample (wherein standard Newtonian mechanics applies). The elliptical stadium function $f$ is zero inside and $0<f<1$ outside:

$$f(x,y)=\min\left[1,\max\left(0,\frac{(x/L_x)^2+(y/L_y)^2-(a/L_x)^2}{1/4-(a/L_x)^2}\right)\right], \tag{1}$$

where $L_x$ and $L_y$ are the width of the entire computational cell and $a$ and $b$ are the $x$ and $y$ axes of the inner sample region, such that $a/L_x=b/L_y$. The maximum damping coefficient, which at zero thermal bath temperature ($T_0=0$), critically damps sound waves at the root-mean-square Einstein frequency $\omega_E$, is given by

TABLE I. Sound speeds in units of $(\epsilon/m)^{1/2}$ for the Morse potentials [see Eq. (4)] and in nm/ps for the Ni-EAM and the harmonic potential.

| Potential | $c_L$ | $c_t$ | $c_R$ |
|---|---|---|---|
| Morse ($\alpha=7$) | 10.5 | 6.1 | 5.6 |
| Morse ($\alpha=6$) | 9.0 | 5.2 | 4.8 |
| Ni-EAM $\langle 100\rangle$ | 5.1 | 3.8 | 2.6 |
| Harmonic $\langle 100\rangle$ | 7.6 | 5.3 | 4.1 |

$$\zeta = 2\omega_E(1-T_0/T)f. \tag{2}$$

The temperature $T$ in the reservoir region is measured as

$$kT = \sum m(u^2+v^2)f \Big/ \left(2\sum f\right),$$

where the sum is taken over all $N$ atoms. If the viscous damping coefficient $\zeta$ is properly tuned to the vibrational spectrum of the model as described by Eq. (2), the ramped viscous damping has been shown[14] to effectively absorb outgoing elastic waves (phonons) of almost all wavelengths. By surrounding the central elliptical sample with this damping reservoir, the vibrational properties of our computational cell are effectively those of an infinitely large system. An atomically sharp crack is embedded in the center of the computational cell, with relaxed atomic displacements, given by the linear elastic solution for such a crack of finite length in an infinite body under uniaxial tension. The whole system is initially displaced such that the elastic solution gives an energy release rate per unit length of crack extension $G$ equal to the surface energy $2\gamma$ of the two crack surfaces, i.e., at the Griffith load $G=2\gamma$. During the simulation the system is further expanded adiabatically and homogeneously normal to the crack plane at a strain rate given by

$$\dot{\varepsilon}(t) = \frac{\dot{\varepsilon}(0)}{1+\dot{\varepsilon}(0)t}. \tag{3}$$

This allows us to drive a crack with very gentle overloading and without the complication of strong loading waves generated when strain or stress is applied only at boundaries.

The interatomic interaction is modeled with various Morse potentials of the form

$$\phi(r) = \epsilon(e^{-2\alpha(r/r_0-1)} - 2e^{-\alpha(r/r_0-1)}), \tag{4}$$

where $r_0$ is the minimum of the potential, $\epsilon$ is the bond strength, and $\alpha$ characterizes the anharmonicity of the potential, which is, for example, reflected in the linear $\alpha$ dependence of the Grüneisen constant or the pressure derivative of the bulk modulus. To make both the potential energy and the force decay smoothly to zero at $r=r_{\max}=2.5r_0$, we multiply the Morse potential [Eq. (4)] with a cutoff function

$$f_{\rm cut}(r) = \left[1-\left(\frac{r-r_0}{r_{\max}-r_0}\right)^3\right]^2 \quad \text{for } r_0<r<r_{\max}. \tag{5}$$

Three sound speeds—longitudinal $c_L$, transverse $c_t$, and Rayleigh $c_R$—are given in Table I; the computational time step in the centered-difference integration of the MD equations of motion was chosen to be $\Delta t=0.02t_0$, where $t_0$ is defined as $r_0\sqrt{m/\epsilon}$. To compare with the results from strip geometry, we choose the unit of time to be $r_0/c_L$ rather than $t_0$. In this paper, we will concentrate on exploring mechanical aspects of dynamic fracture without thermal fluctuations, so we set the initial temperature to nearly zero $(10^{-6}\epsilon/k)$.

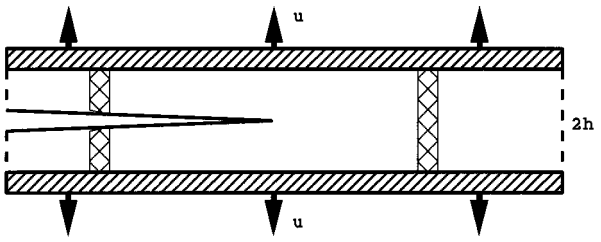


FIG. 2. Schematic outline of the strip geometry in which the central crack can be studied under the condition of constant energy release rate $G$.

The Hamiltonian equations of motion for all $N$ coordinates $\mathbf{r}$ and thermal velocities $\mathbf{v}$ are given by

$$\dot{\mathbf{r}} = \mathbf{v} + \dot{\varepsilon}x\hat{\mathbf{x}}, \tag{6}$$

$$\dot{\mathbf{v}} = \frac{\mathbf{F}}{m} - \dot{\varepsilon}v_x\hat{\mathbf{x}} - \zeta\mathbf{v}, \tag{7}$$

where $\dot{\varepsilon}$ is taken from Eq. (3) and $\zeta$ is the viscous damping coefficient [Eq. (2)] for the ''stadium.'' It seems worth emphasizing again that the center of the stadium is free of any viscous damping, and Newtonian mechanics applies around the crack.

From the Griffith fracture relation $K_{Ic}=2\sqrt{\varepsilon\mu(1+\nu)}$, where $\mu$ is the shear modulus and $\nu$ is Poisson's ratio, the critical strain $\varepsilon_c$ required to propagate the crack is 0.005 for $\alpha=7$ and initial crack length $l_c=240$. For crack growth and dislocation nucleation, we can simulate similar physical processes to those in conventional experiments, provided that the overloading strain changes much slower than the process of crack motion and dislocation emission. For example, with $\dot{\varepsilon}=0.0001$, a pair of atoms separated by one lattice spacing $r_0$ will increase its separation by $0.0001r_0$ in the time period of $t_0$, as compared to the much larger distance that the crack tip runs (about $2r_0$ under a typical maximum crack-tip velocity).

By the use of large computational systems and with the application of the linear elastic solution as initial and boundary conditions, we can study dynamic crack-tip processes in ''realistic'' (i.e., macroscopic) stress and strain fields. In these studies, we are naturally limited to rather short simulation times since the running crack will eventually feel and (sometime later) hit the border of the stadium.

### B. Strip geometry

A different route is followed with the thin strip geometry. Here the crack field is constrained within a thin strip of height $2h$ which is clamped on the top and the bottom by fixed (uniform) displacement boundary conditions (see Fig.

2). By making the strip very long, the dynamically running crack can be followed for rather long times. Furthermore the strip geometry permits us to investigate dynamic crack propagation under the condition of constant energy release rate $G$ (see Refs. 1, 17, and 18). Consequently, long-time steady-state crack propagation may be achieved.

The half-height of the model is chosen to be $h \geqslant 25$ lattice parameters; the length $L$ of the strip is always $L > 8h$, with the crack initially placed at $L/4$. Ramped viscous damping, similar to the method described for the stadium, is applied in the regions adjacent to the upper and lower boundaries as well as at the free surfaces to the right and the left of the model in Fig. 2. The viscous ramp is applied over a distance of 5–10 lattice parameters. Consequently, the vibrational properties of the system are essentially those of an infinitely large system, although the crack field is that of a very thin strip.

Crack propagation in the strip geometry is studied exclusively on the {100} plane of the fcc crystal lattice. Periodic boundary conditions of minimal periodic length are applied along the crack front to model plane strain boundary conditions. The restrictions imposed through the application of periodic boundary conditions are probably of less importance for the analysis of brittle crack propagation but will severely curtail the possibility of dislocation generation. Whereas dislocations could be generated in the form of dislocation loops in a real crystal, here they must be infinitely long and straight. Additional restraints to dislocation emission may result from the geometry of the crack system in relation to the slip systems: Depending on the orientation of the crack front, the natural Burgers vectors can be completely suppressed. Using these features of the periodic boundary conditions, one can therefore study brittle crack propagation in an otherwise ductile material. In this study, the crack front is oriented either along a $\langle 001 \rangle$ direction or along $\langle 011 \rangle$. The crack systems, specified by the crack plane and the crack front direction, are therefore denoted as (100)[001] and (100)[011]. In the (100)[001] crack system, the natural glide planes of the fcc crystal, the {111} planes, are all inclined against the crack front and dislocation emission on these planes is therefore suppressed. Dislocations which could possibly be generated are either of the Lomer type, with a $\langle 001 \rangle$ Burgers vector, or must have larger Burgers vectors. The second crack system provides two sets of {111} glide planes at 54° to the crack plane. The orientation of the $1/6\langle 211 \rangle$ partial dislocations, which could be emitted on these glide planes is such that the edge partial is leading in backward orientation and the 30° partial is leading in the forward direction (see also Ref. 19).

Both these crack systems have already been studied quite extensively in molecular statics simulations of brittle fracture processes and dislocation nucleation.[19,20] The static calculations showed that brittle crack propagation on the original (100) crack plane is expected for both crack systems under opening (mode I) loading conditions for EAM-Ni.[19]

The interatomic interaction is modeled either by an embedded atom (EAM) potential which is fitted to the cohesive energy, the lattice parameter, and the elastic constants of Ni (Ref. 21) or by a fully harmonic nearest-neighbor (snapping-spring) force law. The pairwise harmonic interaction is also fitted to the lattice parameter and the cohesive energy of Ni and goes to zero exactly halfway between first and second nearest neighbors. The sound speeds of these models are also given in Table I.

The MD technique employed here is again a central-difference integration scheme. However, a *local* temperature control,[22] which resembles an electronic heat bath for the ions, is employed to quickly establish steady-state conditions for the running crack. The equation of motion is given by

$$\ddot{\mathbf{r}}_i = \frac{\mathbf{F}_i}{m_i} - \zeta_i \dot{\mathbf{r}}_i \tag{8}$$

with

$$\zeta_i = \zeta_0 \left( \frac{1 - T_0/T_i}{[1 + (\delta T/T_i)^2]^{1/2}} \right),$$

where $\zeta_i$ is a local version of Eq. (2), $T_0$ is the temperature of the electronic heat bath, and $T_i$ is the kinetic temperature of particle $i$. The small term $\delta = 0.1$ K is introduced to keep $\zeta_i$ finite for atoms at rest. The viscous damping coefficient $\zeta_0$ here is usually chosen to mimic the electron-phonon coupling of Ni.[22] To study the influence of the local damping on the behavior of the crack, the damping coefficient is sometimes also decreased to 1/30 of this value. In the ramped viscous damping regions at the outer borders of the model, $\zeta_0$ is gradually increased and $T_0$ is decreased to produce a phonon-absorbing reservoir.

The models are first relaxed at boundary displacements which correspond to the Griffith load, $G_0$, i.e., at boundary displacements which (in front of the crack tip) lead to a homogeneous strain energy per unit length large enough to balance the surface energy of the two crack surfaces. At this load the model is then equilibrated for 20 ps at a temperature of $T_0 = 10$ K. This temperature is also kept as the temperature of the electronic heat bath during subsequent crack propagation. The models are then loaded to a higher strain level by scaling all atomic *displacements* relative to the ideal crystal positions. This scaling is applied instantaneously between two MD steps. Such scaling of the atomic displacements does not change the overall shape of the elastic strain field. The scaling therefore instantaneously changes the load level without creating any shock waves or otherwise disturbing the crack field. Such rescaling of the displacements can in principle be used any time during a MD run to either increase or decrease the load level.

### C. Crack-tip position and velocity

Crack-tip position is determined by inspecting the atomic coordinates or potential energies of the atoms above and below the crack plane. Coming from the intact material, we search for the first pair of atoms which either exceeds a critical opening displacement or which has a potential energy above a certain level. Both the displacement and the potential energy criterion can be tuned such that the ''standard'' pair of crack-tip atoms just fulfills this criterion. Both criteria work equally well and the crack-tip position can usually be determined to within less than one nearest-neighbor distance. If the crack-tip position is determined in this way at every MD time step it remains virtually constant for a certain period of time after which it suddenly jumps to the next pair of

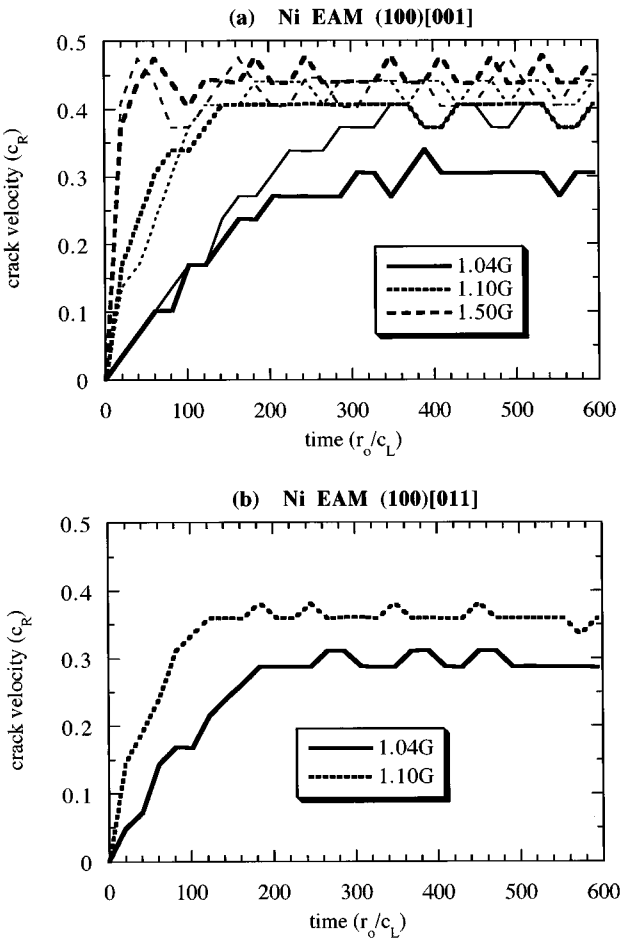


FIG. 3. Crack-tip velocity (in units of Rayleigh wave speed $c_R$) vs time (in units of nearest neighbor distance $r_0=2.49$ Å divided by longitudinal velocity $c_L$) for the EAM-Ni (100)[001] (a) and (100)[011] (b) fcc crack systems at different load levels (in units of Griffith load $G$), as indicated in the legend. For the (100)[001] crack system, the damping coefficient for Ni (heavy lines) as well as a damping coefficient reduced by a factor of 30 (light lines) is used.

atoms. However, the atomic coordinates are usually not inspected at every time step but in larger time intervals $\Delta t_{\text{out}}$ of the order of 10 vibrational periods $\tau_E=2\pi/\omega_E$. Consequently, the crack-tip velocity $v_{\text{tip}}$, determined as the change in crack-tip position divided by the output time interval, $v_{\text{tip}}=\Delta x_{\text{tip}}/\Delta t_{\text{out}}$, is slightly oscillating due to the discretization in time and space, even for perfect steady-state crack propagation (see, for example, Fig. 3). To make the different crack systems comparable, all measured velocities are normalized with respect to the appropriate Rayleigh wave velocities given in Table I.

## III. RESULTS AND DISCUSSION

We divide the presentation of our results and discussion in two parts. In the first part we investigate the perfectly brittle crack propagation, and the second part concentrates on crack tip instabilities which occur for cracks which are sufficiently overloaded.

TABLE II. Maximum crack-tip velocity $v_{\max}$ ($c_R$=Rayleigh wave speed), for various Morse potential parameters $\alpha$, ratios of crack size to sample area $\eta$, and strain rates $\dot{\varepsilon}$.

| | $l_c/r_0\ (t=0)$ | $\varepsilon_0$ | $\alpha$ | $\eta$ | $\dot{\varepsilon} r_0/c_L$ | $v_{\max}/c_R$ |
|---|---|---|---|---|---|---|
| No branching | | | | | | |
| *A* | 480 | 0.0035 | 7 | 5.02 | $5\times10^{-7}$ | 0.180 |
| *B* | 480 | 0.0035 | 7 | 4.19 | $1\times10^{-6}$ | 0.261 |
| *C* | 240 | 0.005 | 7 | 1.05 | $1\times10^{-5}$ | 0.342 |
| Branching | | | | | | |
| *D* | 240 | 0.005 | 7 | 1.05 | $5\times10^{-5}$ | 0.360 |
| *E* | 240 | 0.0058 | 6 | 1.05 | $5\times10^{-5}$ | 0.356 |
| *F* | 240 | 0.0058 | 6 | 1.05 | $1\times10^{-5}$ | 0.356 |

### A. Brittle dynamic fracture

The propagation of perfectly brittle atomically sharp cracks is mainly studied in the thin strip geometry. The dependence of the crack tip velocity on the overload is displayed in Fig. 3 for different load levels and the two different damping coefficients. For both crack systems, the plot of the crack tip velocity versus time [Figs. 3(a) and 3(b)] shows that the crack tip accelerates to a terminal steady-state velocity. The acceleration implies a very small but finite inertia of the crack in the given geometry. If the energy release rate above the Griffith load is interpreted as the driving force for the crack, the inertia does not depend on the load level or the damping coefficient.

The terminal velocity reached at the different load levels shows some interesting aspects. At small overloads, between $1.00G_0$ and $1.02G_0$ the crack is stationary due to lattice trapping in both crack systems. At $1.04G_0$ the crack starts to move and accelerates up to a terminal velocity which already is a sizable fraction of the Rayleigh wave speed. With only a very small local viscous damping [light curve in Fig. 3(a)] the lowest steady-state crack-tip velocity is already as high as approximately $0.3c_R$. This suggests that the steady-state propagation of a perfectly brittle crack at very low temperatures is limited to velocities above a certain lower critical value, which has previously been found[5] in experiments and has been discussed[11,12] in simple analytical 2D crack models. Our MD study, at least on time scales accessible to us, seems to be consistent with these. The precise physical interpretation of the origin of this forbidden band of low velocities, however, still remains unclear.

Studies with the stadium boundary conditions can give some additional information as far as this ''forbidden'' band of lower velocities is concerned. We have performed calculations with various initial crack lengths $l_c(t=0)$, strain rates $\dot{\varepsilon}$, and Morse potential parameters $\alpha$. We emphasize two principal observations: (1) decreasing $\alpha$ tends to make dislocation emission easier and (2) increasing $\dot{\varepsilon}$ causes a crack to branch sooner and makes its branching paths more chaotic. Table II gives the maximum crack-tip velocities for various strain rates and ratios $\eta$ of crack size to sample area $S$: $\eta=2\pi l_c^2(t=0)/S$.

We find that the maximum velocities increase with decreasing ratios of crack size to sample area. It is interesting to note that no branching is observed below $\sim 0.35c_R$.

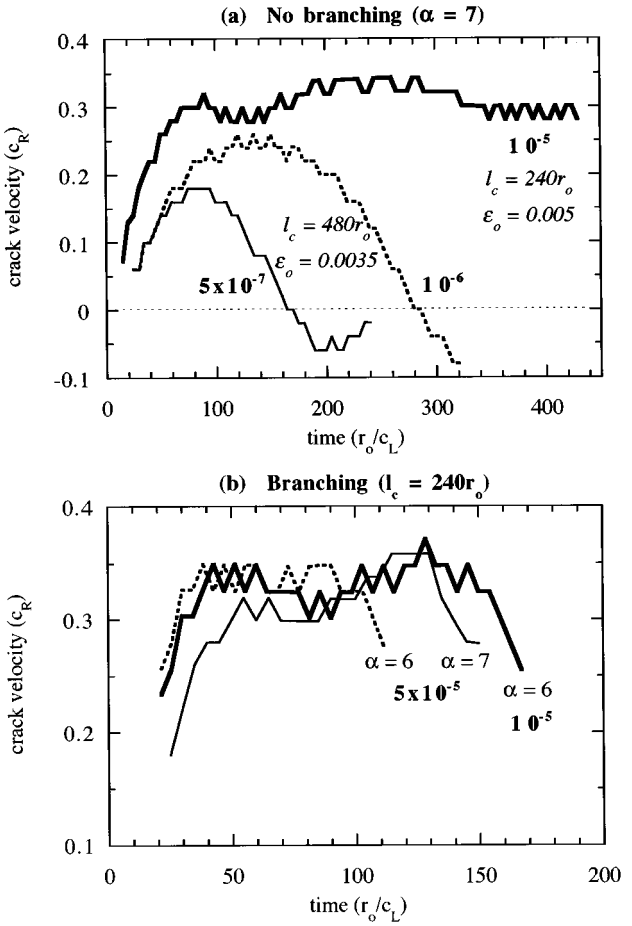


FIG. 4. The crack-tip speed (in units of Rayleigh wave speed $c_R$) as a function of time (in units of nearest-neighbor distance $r_0$ divided by sound speed $c_L$) for the stadium geometry. Strain rate (bold label) is in units of $c_L/r_0$. (a) without crack branching, (b) with crack branching.

We would like to point out that our viscous damping boundary is able to effectively absorb the outgoing waves generated from the dynamic crack-tip but not to prevent incoming waves from fixed displacement boundaries. Therefore a new dynamic crack stress field is established corresponding to the clamped boundary condition. The farther the crack tip propagates, the more the actual (instantaneous or transient) crack-tip stress field deviates from the initial crack stress field of the infinite solid. It is known that the stress intensity factor decreases as the crack propagates in a ''fixed grip'' boundary condition. If the loading rate is high enough, however, the resulting stress intensity factor can stay almost constant or increase. We are thus able to fine-tune the dynamical crack behavior through the specimen geometry factor $\eta$ and loading rate $\dot{\varepsilon}$. Our simulation results follow the above predictions. In Fig. 4, we present some of our results for crack-tip velocities as a function of time. Figure 4(a) shows cases where no crack branching was observed. For case $A$ in Table II, the crack starts to run, reaches the maximum velocity, goes to zero velocity at $t=180$, then starts to retreat, and at $t=255$, moves forward again. With twice the loading rate (case $B$), we see similar features except that the maximum crack-tip velocity increases from $0.18c_R$ to $0.26c_R$ and the crack runs farther. Crack arrest appears to be caused by our ''fixed grip'' loading. With the appropriate combination of short initial crack length and high loading rate (case $C$), we can realize relatively stable crack propagation at almost constant velocity (around $0.34c_R$) for a fairly long time. The terminal velocity is similar in magnitude to that seen in the strip geometry discussed above. It is, however, significantly lower than the Rayleigh wave speed which is the terminal velocity according to continuum analysis.[1] This aspect will be discussed in more detail below.

Now we will discuss the effect of viscous damping on dynamic cracks. As shown in Fig. 3, the terminal steady-state velocities decrease with increasing viscous damping, in particular at small overloads. The damping coefficient acts locally and most strongly on the atoms with the highest velocities. In this sense the local damping could be interpreted as reducing the amplitude of the shear waves carrying the information that the crack is propagating. The damping would thereby essentially reduce the apparent overload and therefore reduce the steady-state crack-tip velocity. The effect of viscous damping on crack-tip velocity is, however, not fully clarified yet.

Upon increasing the load to a value of $1.10G_0$, the crack reaches a terminal velocity of about $0.4c_R$. Further increasing the load up to $1.50G_0$ for the (100)[001] crack system (see Fig. 3) or to $1.30G_0$ for the (100)[011] crack system (see Fig. 3) does not significantly change the terminal velocity. Furthermore, the crack-tip velocity is almost independent of the damping coefficient in this loading regime. Averaged over longer times the steady-state crack-tip velocity is even somewhat lower for the lower damping coefficient at $1.50G_0$, which may be seen as an indication of the approach to the critical overload of this system. This issue will be discussed further in the second part of this section.

Here, however, one should ask how the crack manages to travel at almost identical velocity but to dissipate such different amounts of energy. An answer may be found by analyzing the velocity fields around the crack tips moving at the same steady-state velocity at overloads of $0.10G_0$ and $0.50G_0$. For the (100)[001] crack system these velocity fields are displayed in Fig. 5. At small overloads the velocity field around the crack is smooth and continuous as expected from continuum theory. At increasing overloads, however, the crack creates a ''shock wave'' at the breaking of every single atomic bond. This acoustic emission is mainly of longitudinal compressive character in the direction perpendicular to the crack plane with a significant transverse component at an angle of 45° to the crack propagation direction. No such acoustic waves are visible in the angular section between about $-45°$ and 45° around the crack propagation direction.

To better understand the origin of these acoustic waves one can investigate the instantaneous crack-tip configurations, one of which is shown in Fig. 6(a) halfway between the breaking of the last and the next bond at the crack tip during steady-state propagation. It is clearly seen that the atoms above and below the actual crack-tip have been pushed far away from the two crack tip atoms. Such behavior can be rationalized as a consequence of the nonlinearity of the interatomic interaction, which strengthens in compression and weakens in tension. The last broken bond obviously caused the atoms, which are now just behind the crack tip, to impact into the surface, thereby pushing their neighbors with

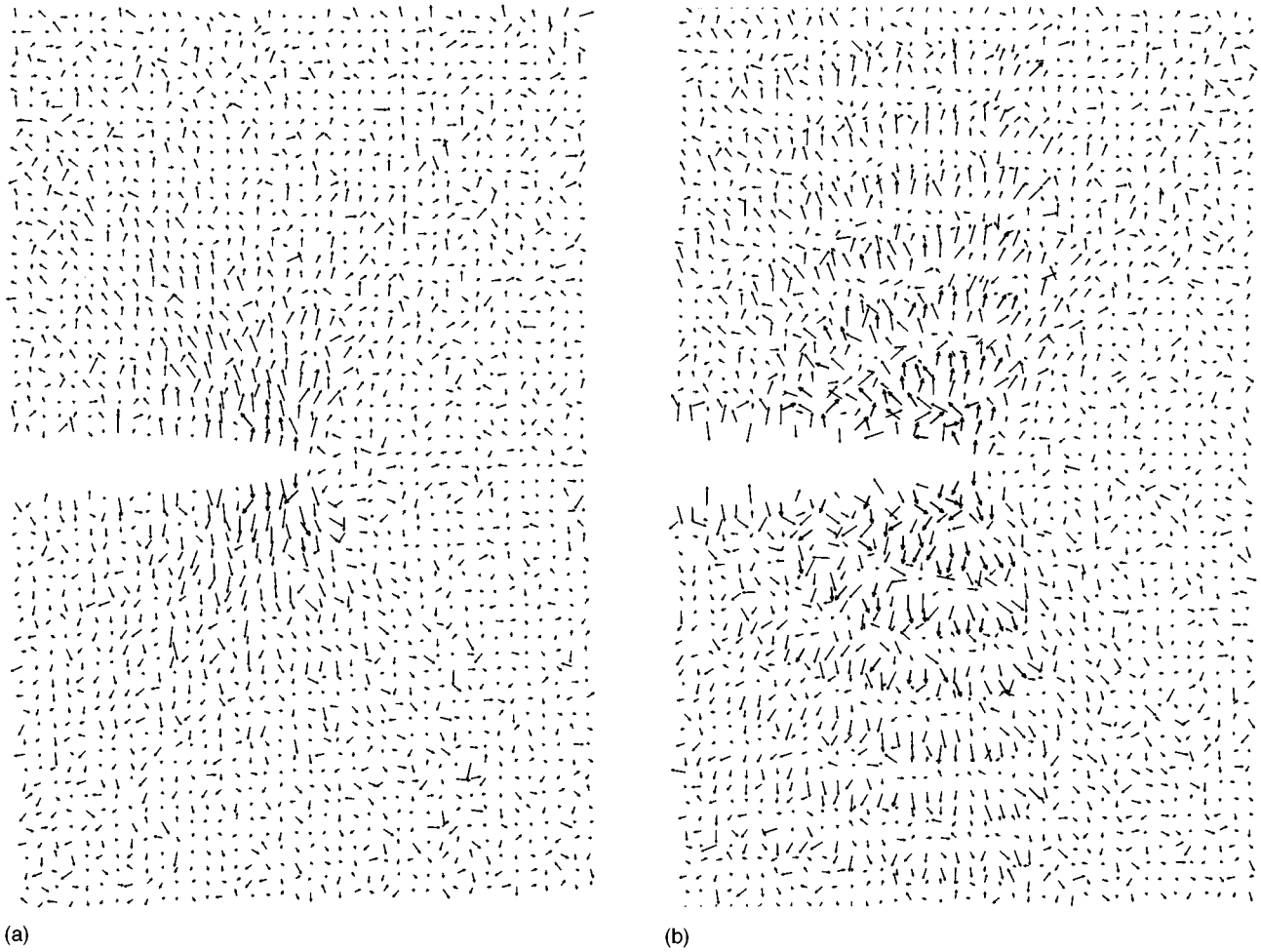


FIG. 5. Velocity distribution of individual atoms around two (100)[001] cracks moving at the same steady-state velocity but subjected to different overloads: (a) $\Delta G = 0.1G_0$, (b) $\Delta G = 0.5G_0$.

strong compressive forces into the crystal. The interatomic interaction of the impacting atoms and their neighbors with the crack-tip atoms thereby weakens due to the nonlinearity of the interatomic potential. The reduced coupling strength in turn reduces the velocity at which information is transferred along the crack surface. Thus, nonlinearity is shown to be responsible for the rather low terminal steady-state velocity as compared to continuum analysis.[1] This result can also be reproduced by a simple one-particle model for crack propagation.[23]

The hypothesis that the nonlinearity of the interatomic interaction is responsible for the rather low terminal crack-tip velocity of the moving brittle crack can be tested by repeating the dynamic calculations with the simple harmonic pairwise snapping spring force law. These simulations are rather difficult since the short-range snapping spring force law results in a rather large lattice trapping of $\Delta G > 1.0G_0$. Furthermore second neighbors may come within interaction range and make the effective interaction nonlinear. To circumvent these difficulties, the neighbor list of the atoms is frozen in the initial configuration and not updated during crack propagation. To start the crack, it was loaded beyond the lattice trapping range for only 1 ps and then instantaneously unloaded to much smaller overloads, whereby it could then reach the steady state. One then finds that it is possible to drive the perfectly brittle crack up to 0.85 of the Rayleigh wave speed at very moderate overloads of only $0.40G_0$. The resulting velocity distribution around the running crack tip is shown in Fig. 7. It clearly reveals the perfectly continuous velocity distribution expected from continuum theory and shows no signs of any acoustic emission from bond breaking (although one might have guessed that the extremely nonlinear snapping of the bonds could have caused such behavior).

### B. Dynamic instability

Driving the crack at higher loads results in crack-tip instabilities. The loads necessary to create an instability depend quite strongly on the actual crystallographic orientation and on the viscous damping. For the strip geometry and the (100)[001] crack system studied above, the critical load is approximately $1.9G_0$ (if the damping coefficient for Ni is used) and only about $1.7G_0$ for the reduced damping. The (100)[011] crack becomes unstable already at a load of $1.4G_0$.

Upon increasing overload, the instability event for the (100)[001] crack of Fig. 6 beyond the steady-state regime is mainly transverse shearing of the {110} planes at 45° into ⟨110⟩ directions. Despite the large shear on these planes (see

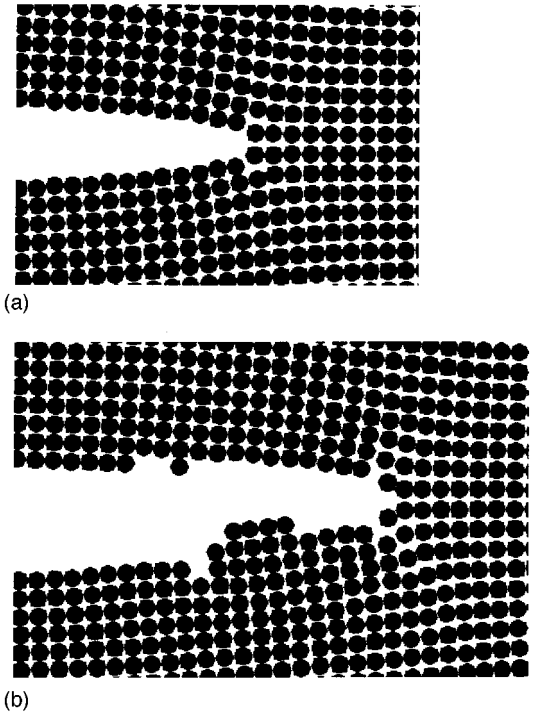


FIG. 6. Snapshot of the atomic configurations at the tip of a ''shock-wave'' emitting (100)[001] crack at $G=1.5G_0$ halfway between the breaking of the last atomic bond and the next (a) and at $G=2.0G_0$ after the generation of a cleavage step (b).

Fig. 5), dislocations of such large $\langle\overline{1}10\rangle$ Burgers vectors at first cannot successfully be created. Similarly, dislocations with [100] Burgers vectors normal to the crack plane are not observed and the overload is not large enough to allow for bifurcations. As a consequence, the crack tip which is just going unstable at a load of $2.0G_0$ has only two possibilities: it can either create a Lomer dislocation with a Burgers vector parallel to the crack propagation direction (as is occasionally observed), or it can attempt to branch. Such branching attempts are seen most often. They eventually lead to one or two atomic steps on the fracture surface.

At higher overloads the instability events become even richer. For the same crack-tip orientation larger deflections of the crack are observed in connection with the emission of $\langle 110\rangle$ dislocations and even climb processes can be observed near the crack tip. However, since such behavior occurs under less well-controlled circumstances, we restrict ourselves to the study of the first instabilities encountered after steady-state propagation.

More comprehensive studies of dynamic crack instability can be carried out in the stadium-boundary system. In such a system, we observed the first instability (branching) when the terminal velocity is larger than $0.35c_R$ as shown in Fig. 4(b), where data are plotted up to the initiation of the first branching. It is interesting to note that those speeds with branching are very close to experimental values reported by Sharon *et al.*[7]

As an example we describe in detail case $F$ in Table II, which is plotted as the full line in Fig. 4(b). Here the atoms first readjust their initial positions given by elastic theory. At $t=20$, the crack starts to propagate and quickly reaches the terminal velocity of about $0.356c_R$ at a time of $t=60$. The

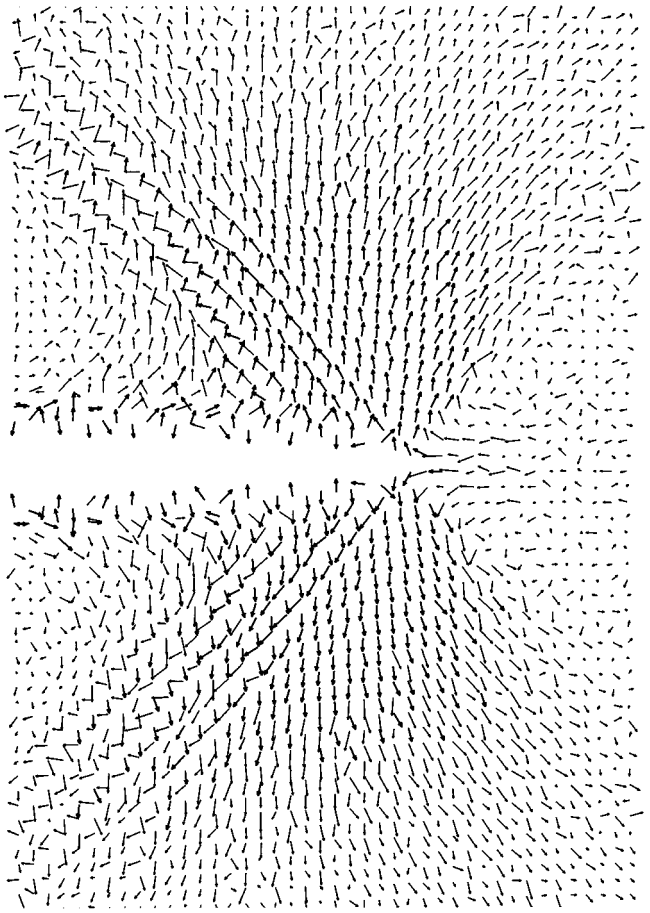

FIG. 7. Velocity distribution around a (100)[001] crack modeled with a harmonic snapping spring force law. The crack is loaded at $G=1.4G_0$, where it reaches a steady-state velocity of $0.85c_R$.

dynamic crack has been unsuccessfully attempting to branch, which causes the small oscillation of the crack-tip velocity. As it opens up, the dynamic crack tip gets more rounded in shape than the initial static one; the tendency for the crack to branch increases with time. At $t=220$, the crack loses the stability and branches. Figure 4(b) clearly shows that the branching is a cumulative process, since the crack velocity has reached a relatively steady value after $t\approx 60$. Similar observations have also been made in the strip-geometry system, although high overloading imposed at the beginning of crack propagation shortens the cumulative time for instability.

This finding of a dynamic buildup is different from traditional theories which assume that the crack-tip velocity *uniquely* determines the behavior of a dynamic crack. Furthermore, the crack branching occurs at a significantly reduced velocity than the maximum value. Clearly, the crack-tip velocity is *not* a necessary condition to trigger the crack-branching instability. Instead, we find that the gradual accumulation of energy around the dynamical crack tip is an essential feature for the ultimate emission of dislocations and crack branching.

We find that local potential energy is the most useful way to show defect configurations such as crack surfaces and dislocation cores. As seen in Fig. 8, local potential energy clearly indicates the future growth paths of cracks or dislocations. In Figs. 8(a)–8(d), we see clearly the buildup of the

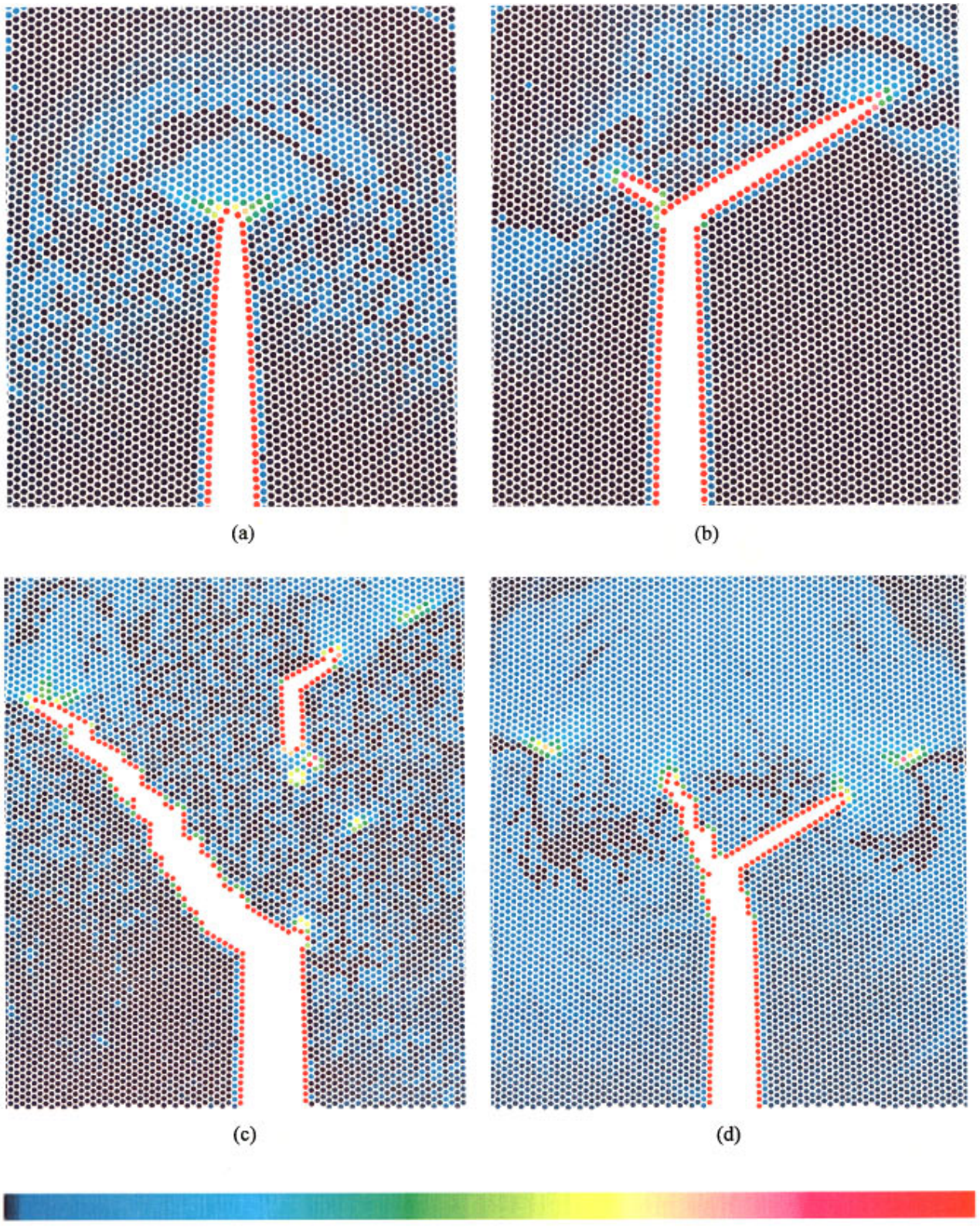


FIG. 8. (Color) Crack configurations following brittle phase of propagation where atoms are colored according to their potential energies by a rainbow ranging from deep blue for a minimum value of $-3.0$ (bulk) to bright red for a maximum value of $-2.0$ (free surface), indicated by the color bar. (a)–(d) are for cases $F$, $E$, and $D$ (see Table II): (a) A dislocation has nucleated at the crack tip on the $-60°$ slip plane ($t=215$) for case $F$; (b) the $-60°$ branching crack closely follows the dislocation and grows at $t=380$; and similarly another branching crack is created after a dislocation is emitted along $+60°$ (for case $F$); (c) $t=440$ for case $E$; (d) $t=305$ for case $D$.

potential energy associated with the phonon field, and we see that dislocations can be emitted from a ''brittle'' crack tip (defined here as a static crack tip that cannot emit a dislocation) when the crack runs sufficiently fast. Therefore, crack motion promotes dislocation emission. The energy buildup around the dynamic crack and the causes of dynamic dislocation emission are discussed in detail in Refs. 24 and 25.

We find that crack branching is closely tied to dislocation nucleation and emission. In Fig. 8(a), one dislocation has nucleated at the right side of the crack tip (at $t=215$). Then it is ejected $2r_0$ away from the crack tip along the $-60°$ slip plane. At $t=250$, the crack tip starts to branch along the same slip plane as the emitted dislocation, and the branch closely follows the dislocation motion. A similiar process of dislocation emission and crack branching also happens along the $+60°$ slip plane a little bit later (around $t=265$) [see Fig. 8(b)]. These general features were observed by Holian and Ravelo[14] though admittedly under much cruder loading conditions than ours. Ohr and his co-workers[26] have observed this same phenomenon in their TEM experiments.

As seen in Fig. 8(b), asymmetric branching can occur. This is understandable: the 2D triangular lattice is macroscopically isotropic, but not locally. The $+60°$ and $-60°$ slip planes are not symmetric relative to a crack tip, so it is impossible for a crack to branch completely symmetrically — the choice of path is made randomly. Once the crack tip has begun to branch along one of the two slip planes, the accumulated energy at the crack tip has been partially released, so that the possibility of growing immediately along the other slip plane is suppressed.

To see the effect of loading rate on branching, we increased $\dot{\varepsilon}$ from $10^{-5}$ to $5\times10^{-5}$. Although the branching pattern has changed significantly [see Fig. 8(c)], the mechanism is still the same. The crack achieves the instability sooner (about $t=150$) because of the increased flux of external energy into the system. The dislocation emission along $+60°$ triggers crack branching in that direction. However, the crack changes its path to $0°$ again, and then switches back to $60°$. It repeats this zigzag, emitting dislocations as time goes on. It is clear that one dislocation is ahead of this branching crack. The other two emitted dislocations stay about $20r_0$ in front of the main crack, nucleating a vacancy as well as a new crack. This new crack first propagates in the $0°$ direction, then branches along $-60°$ following the dislocation it emits, and finally turns its path to $0°$ again. It changes path right at the core of an incipient dislocation at the tip of this branching crack. Similar results are also observed by changing the Morse parameter $\alpha$ from 6 to 7 [see Fig. 8(d)]. It is also noted that for $\alpha=6$ [see Fig. 8(b)] the branching crack closely follows the emitted dislocation while for $\alpha=7$ [see Fig. 8(d)] the branching crack tip and the emitted dislocation are separated by a few lattice spacings. In all these cases, the crack branching is triggered by dislocation emission, following the motion of the emitted dislocation.

Based on our results, we can now discuss what causes dynamic crack branching. The driving force for dislocation nucleation in a crystal increases with increasing speed. For mode I loading in a 2D triangular lattice, dislocation nucleation occurs preferably along $\pm60°$ (see Ref. 1). Dislocation nucleation distorts the arrangement of the atoms near the slip plane at the crack tip and creates a weak path for the crack to follow, by analogy with the fact that two blocks of crystal are easier to pull apart after they are sheared. Figure 8 clearly shows that dislocation nucleation and mobility determine the initial crack branching path and branching angle, since dislocation nucleation and motion is easier for $\alpha=6$ than for $\alpha=7$ (see Refs. 27 and 28). This argument is also consistent with the observations in the ''strip geometry.'' For those system with $\pm90°$ slip planes, the driving force for dislocation emission in those slip planes are small. So it is hard to nucleate and emit dislocations. Thus the crack branch only extends one or two lattice spacings before turning back to the $0°$ plane, leaving a cleavage step (see Fig. 6).

Once the crack branches and grows a few lattice spacings along the slip planes, the branching cracks gradually change their paths so that the average paths have small angles relative to the original crack path. The distortions of the stress field caused by dynamic cracks gradually fade away; therefore, the stress field approaches the static one, which requires crack growth in the $0°$ plane. The smaller angles of crack branching observed in the experiments are very possibly the average over the whole branching path, rather than the first branching angle, due to the limitation of experimental resolution. This is illustrated by Figs. 8(b)–8(d), where the average angles for the branching crack on the left side of the cracks are $60°$, $\sim40°$, and $\sim25°$, respectively. For comparison, in the work of Xu and Needleman,[13] the average branching angles are about $29°$.

As a last example, the $(100)[0\bar{1}1]$ crack represents a case where the first dislocation emission completely stops the crack. At the first instability, at a load of $1.4\,G_0$, the crack emits a full $1/2\langle110\rangle$ dislocation in the forward direction to one side and a microtwin in the forward direction to the other side. Further increase of the applied load only increases the width of the microtwin and eventually leads to the emission of backward-oriented dislocations but will not allow brittle crack propagation again. The behavior of this crack on a macroscopic length and time scale would be interpreted as ductile response, although the crack initially (or under smaller overload) is able to propagate in a perfectly brittle manner. For the 2D triangular lattice with $3.5<\alpha<5$, we also observed that dislocations are emitted after the crack has propagated a few lattice spacings and then the dynamic crack stops. Holian and Ravelo[14] have reported that for Lennard-Jones (LJ) 6-12 (similar to the Morse potential with $\alpha=6$), dislocation emission did stop the crack, but only momentarily. The crack resumes its propagation when it is under sufficiently high loading. Dislocation emission and crack propagation repeats until branching finally occurs. This observation could be due to the strong overloading condition in their simulation. Understanding whether the crack will be stopped by dislocation emission or whether it will further grow (as in the case displayed in Fig. 8) is of course one of the major goals of MD modeling of fracture processes, to be studied in future work.

## IV. SUMMARY

In general, two different simulation systems, stadium boundary and strip geometry, give very similar results. The study of the propagation of brittle cracks shows very close

similarities to experimental observations,[6,7] where the maximum steady-state velocity of such cracks is found to be limited to between 34% (for a 2D triangular lattice and a Morse potential) and 40% of the Rayleigh wave speed (for the (100)[001] crack in EAM-Ni). Cracks release the surplus of mechanical energy by emitting strong acoustic waves at the breaking of every atomic bond, which are caused by the nonlinearity in the interatomic interaction. The nonlinearity of the interatomic interaction is also responsible for the ''low'' terminal velocity, which can be reached by the moving brittle crack.

Our simulations indicate that reaching the terminal crack velocity is *not* sufficient to cause crack branching. This is different from existing continuum and lattice theories, where a critical crack velocity is used as the only indicator for crack branching.[1,12] As shown in Fig. 4 and Table II, a dynamic crack cannot branch when its maximum velocity is below $0.35c_R$. On the other hand, for those cracks with high enough maximum velocity, they do not branch right at the maximum velocity. Instead, branching occurs after the crack passes the maximum velocity and has propagated for a while. Our simulation results suggest that the energy associated with the dynamic crack rather than crack-tip velocity provides a good criterion for describing the crack branching instability.

## ACKNOWLEDGMENTS

Computations were performed on the CM-5 at the Advanced Computing Laboratory at Los Alamos. We also acknowledge helpful discussions with R. Thomson, A. Needleman, R. Ravelo, J. Langer, M. Marder, and R. Blumenfeld. P.G. gratefully acknowledges partial financial support by the KSB-Stiftung, Stuttgart.

*Author to whom all correspondence should be addressed.

[1] L.B. Freund, *Dynamic Fracture Mechanics* (Cambridge University Press, New York, 1990).
[2] J.E. Hack, S.P. Chen, and D.J. Srolovitz, Acta Metall. **37**, 1957 (1989).
[3] E.H. Yoffe, Philos. Mag. **42**, 739 (1951).
[4] W.G. Knauss and K. Ravi-Chandar, Int. J. Fract. **27**, 127 (1985).
[5] J. Fineberg, S.P. Gross, M. Marder, and H.L. Swinney, Phys. Rev. Lett. **67**, 457 (1991).
[6] S.P. Gross, J. Fineberg, M. Marder, W.D. McCormick, and H.L. Swinney, Phys. Rev. Lett. **71**, 3162 (1993).
[7] E. Sharon, S.P. Gross, and J. Fineberg, Phys. Rev. Lett. **74**, 5096 (1995).
[8] J.S. Langer, Phys. Rev. Lett. **70**, 3592 (1993); J.S. Langer and H. Nakanishi, Phys. Rev. E **48**, 439 (1993).
[9] E.S.C. Ching, J.S. Langer, and H. Nakanishi, Phys. Rev. Lett. **76**, 1087 (1996).
[10] B. Cotterell and J.R. Rice, Int. J. Fract. **16**, 155 (1980).
[11] M. Marder and X. Liu, Phys. Rev. Lett. **71**, 2417 (1993).
[12] M. Marder and S. Gross, J. Mech. Phys. Solids. **43**, 1 (1995).
[13] X. -P. Xu and A. Needleman, J. Mech. Phys. Solids. **42**, 1397 (1994).
[14] B.L. Holian and R. Ravelo, Phys. Rev. B **51**, 11 275 (1995).
[15] D.M. Beazley and P.S. Lomdahl, Parall. Comp. **20**, 173 (1994).
[16] F. Abraham, D. Brodbeck, R.A. Rafey, and W.E. Rudge, Phys. Rev. Lett. **73**, 272 (1994).
[17] P. Gumbsch, in *Computer Simulation in Materials Science: Nano/Meso/Macroscopic Space and Time Scales*, edited by H.O. Kirchner, L. Kubin, and V. Pontikis (Kluwer Academic, Netherlands, 1996), p. 227.
[18] P. Gumbsch, Z. Metallkd. **87**, 341 (1996).
[19] P. Gumbsch, J. Mater. Res. **10**, 2897 (1995).
[20] P. Gumbsch and G.E. Beltz, Model. Sim. Mater. Sci. Eng. **3**, 597 (1995).
[21] S.M. Foiles, M.I. Baskes, and M.S. Daw, Phys. Rev. B **33**, 7983 (1986).
[22] M.W. Finnis, P. Agnew, and A.J.E. Foreman, Phys. Rev. B **44**, 567 (1991).
[23] B.L. Holian, R. Blumenfeld, and P. Gumbsch, Phys. Rev. Lett. **78**, 78 (1997).
[24] S.J. Zhou, P.S. Lomdahl, R. Thomson, and B.L. Holian, Phys. Rev. Lett. **76**, 2318 (1996).
[25] S.J. Zhou, N.G. Jensen, A. Bishop, P.S. Lomdahl, and B.L. Holian (unpublished).
[26] S.M. Ohr, Scr. Metall. **20**, 1501 (1986).
[27] S.J. Zhou, A.E. Carlsson, and R. Thomson, Phys. Rev. B **47**, 7710 (1993).
[28] S.J. Zhou, A.E. Carlsson, and R. Thomson, Phys. Rev. Lett. **72**, 852 (1994).